Int. J. Heat Mass Transfer. Vol. 19, pp. 425–429. Pergamon Press 1976. Printed in Great Britain

UNIVERSAL RELATIONS FOR BUBBLE GROWTH

T. G. THEOFANOUS and P. D. PATEL
Purdue University, West Lafayette, IN 47907, U.S.A.

(*Received* 8 *January* 1975 *and in revised form* 7 *July* 1975)

Abstract—The initial-to-final vapor density ratio, when significantly greater than one, strongly influences vapor bubble growth rates in the inertia and the inertial/heat-transfer regimes. This effect is not predicted by the previous analytical formulation of Mikic, Rosenhow, and Griffith. All published experimental data were obtained at low values of this density ratio and have failed to uncover this omission. The solution shown as a universal plot in Fig. 4 does not bear this deficiency, and is supported by comparisons with new experimental data and detailed numerical simulations.

NOMENCLATURE

A, a parameter, $\left(\frac{2}{3}\frac{\lambda\rho_v^*(P_\infty)(T_\infty - T^*(P_\infty))}{\rho_l T^*(P_\infty)}\right)$;
A_*, a parameter, defined by equation (8);
B, a parameter, defined by equation (9);
c, specific heat;
P, pressure;
$P^*(T)$, saturation pressure at temperature T;
R, bubble radius;
R^*, nondimensional bubble radius, defined by equation (11);
R^+, nondimensional bubble radius, defined by equation (15);
T, temperature;
$T^*(P)$, saturation temperature at pressure P;
t^*, nondimensional time, defined by equation (11);
t^+, nondimensional time, defined by equation (16).

Subscripts

l, liquid;
v, vapor;
∞, conditions far away from the bubble.

Greek letters

α, thermal diffusivity;
β, a parameter, defined by equation (17);
Γ, a parameter, defined by equation (10);
λ, latent heat of evaporation;
ρ, density;
$\rho^*(P)$, saturation density at pressure P;
$\rho^*(T)$, saturation density at temperature T;
ϕ, a parameter, defined by equation (3).

INTRODUCTION

INERTIA and heat transfer are known to represent the primary factors limiting the growth rate of vapor bubbles in superheated liquids. Exact solutions for each of the two asymptotic regimes (considering these rate processes individually) for spherically symmetric growth, and uniform superheat, were obtained by Rayleigh [1], Scriven [2], and Birkhoff *et al.* [3]. For many years the heat-transfer regime remained important as being representative of the practically significant problems. Experimental verification for this regime was reported for a number of fluids and conditions [4]. During the past several years, interest has shifted towards studying the inertia effects. This may be attributed to the increasing importance of liquid metals as heat-transfer media (e.g. in liquid metal cooled fast breeder reactors). In such systems the role of inertia is enhanced due to the diminished effect of heat transport as the rate limiting process. Indeed, many practical as well as diverse problems in liquid metal systems are reduced to vapor bubble growth in the combined inertial/heat-transfer regime. For example, Bankoff and Fauske [5] have thus studied boiling transition. Other applicable situations may be found in [6].

Numerical [7–9] as well as experimental [9, 10] studies established the existence, importance, and mathematical modelling of the combined regime. However, only through the work of Mikic *et al.* [11] did it become possible to obtain a comprehensive and convenient analytical solution. We will refer to it as the MRG solution. Excellent agreement with the experimental data of Lien [10, 11] and Board and Duffy [9] has been reported. In comparing the MRG solution to our own experimental data [12, 13] however, discrepancies were noted. For certain experimental conditions they were excessive; for others, very good agreement was observed. To further verify these conclusions, comparisons with "numerical bubble growth experiments" were made. A previously presented [8] mathematical model was utilized to generate these numerical "data". The same trends were noted. An illustration is provided in Fig. 1. The MRG solution is seen to underpredict the experimental growth rate of Run 55-G36, while good agreement between the experimental data and the numerical solution is observed. Clearly, an effect not accounted for in the MRG formulation is active for the experimental conditions of Run 55-G36. This conclusion, in effect, disputes the universality of the MRG solution suggested through the comparisons with previous experimental data. It is the purpose of this paper to show that an additional dimensionless grouping must enter the formulation in order to achieve a universal representation. Only the case of uniform superheat will be considered here.

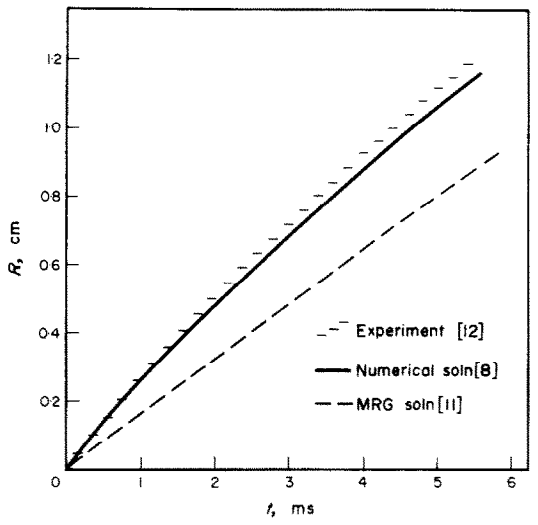

FIG. 1. A comparison of the MRG and numerical solutions with experimental data (run 55-G36, Freon-113, superheat = 107°F, $T_\infty = 73$°F).

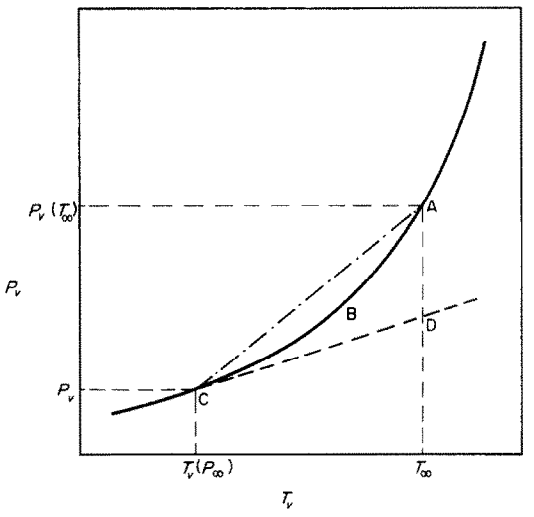

FIG. 2. Qualitative comparison of the $P_v - T_v$ assumptions.

FORMULATION

The overall approach and the basic initial assumptions of Mikic *et al.* [11] will be adopted here. The matching of the two asymptotic regimes (inertial and heat-transfer) is accomplished by considering the two corresponding rate equations as a system:

$$\frac{dR}{dt} = \sqrt{\left[\frac{2}{3}\frac{P_v(t) - P_\infty}{\rho_l}\right]} \tag{1}$$

$$\frac{dR}{dt} = \left(\frac{12}{\pi}\alpha_l\right)^{1/2} \frac{\rho_l c_l (T_\infty - T_v(t))}{\lambda \rho_v} \frac{}{2\sqrt{t}} \tag{2}$$

The vapor is assumed saturated and in equilibrium with the bubble wall liquid. This provides a relationship between P_v and T_v. They can thus be eliminated in order to obtain the rate of growth as a function of time. In the MRG solution this was accomplished by using the linearized Clausius–Clapeyron for $P_v(t)$ and assuming a constant vapor density (ρ_v) evaluated at P_∞. The implications of these two choices can be explained with reference to Fig. 2. The solid ABC line on this figure represents the vapor pressure curve. Point A represents the initial state and point C the final state which is approached asymptotically. During the growth process the vapor state is described by a point moving monotonically from A to C. The line CD represents the type of linearization utilized in the MRG solution. It is seen that as the superheat, $\Delta T_s = T_\infty - T_v^*(P_\infty)$, increases, the vapor pressure is underestimated for greater portions of the growth and by increasing amounts. This leads to an underestimation of the growth rate given by equation (1). On the other hand the vapor density at point C, $\rho_v^*(P_\infty)$, underestimates the actual vapor density found along ABC. This leads to an underestimation of the latent heat requirements and hence, through equation (2), to an overestimation of the growth rate. Again the error increases with superheat. Both these errors are small only for very low superheats. This condition, however, negates the need for the solution sought, since the heat-transfer asymptotic regime is then found adequate.

The effort in the present analysis will be to correctly represent vapor pressures and vapor densities at both end points of the process (A and C). Even a linear interpolation (see Fig. 2) should yield a better approximation of the process as a whole. Clearly more elaborate schemes are possible. The gained incremental accuracy, however, does not appear to justify the incremental inconvenience and loss of clarity in the final results. Now both the pressure and the density are overestimated leading to an overestimation of the rate in equation (1) and an underestimation in equation (2).

The factor ϕ reflecting the loss in driving force may be defined by:

$$\phi^2 = \frac{T_v - T^*(P_\infty)}{T_\infty - T^*(P_\infty)}. \tag{3}$$

The linear interpolations for P_v and ρ_v discussed above may be written as:

$$P_v - P_\infty = P_v^*(T_v) - P_\infty = (P_v^*(T_\infty) - P_\infty)\phi^2 \tag{4}$$

$$\rho_v - \rho_v^*(P_\infty) = \rho_v^*(T_v) - \rho_v^*(P_\infty) = (\rho_v^*(T_\infty) - \rho_v^*(P_\infty))\phi^2. \tag{5}$$

Equations (1) and (2) then become:

$$\frac{dR}{dt} = A_*\phi \tag{6}$$

and

$$\frac{dR}{dt} = \frac{B}{2}\frac{1-\phi^2}{[1+(\Gamma-1)\phi^2]\sqrt{t}} \tag{7}$$

where:

$$A_*^2 = \frac{2}{3}\frac{P^*(T_\infty) - P_\infty}{\rho_l} \tag{8}$$

$$B^2 = \left(\frac{12}{\pi}\alpha_l\right)\left\{\frac{\rho_l c_l (T_\infty - T^*(P_\infty))}{\lambda \rho_v^*(P_\infty)}\right\}^2 \tag{9}$$

and

$$\Gamma = \rho_v^*(T_\infty)/\rho_v^*(P_\infty). \tag{10}$$

The grouping B is the same as that of the MRG solution.

The A_* differs from the A of MRG in that it represents the *exact* maximum available pressure driving force. The grouping Γ represents a new effect not present in the MRG solution. It increases with superheat but the rate of increase depends on the substance and the absolute pressure level. From the combination of A_*

RESULTS AND DISCUSSION

The function $\phi = \phi(t^*; \Gamma)$ is obtained by solving, for various values of Γ, the algebraic equation:

$$\frac{\phi}{1-\phi^2}[1+(\Gamma-1)\phi^2] = \frac{1}{2\sqrt{(t^*)}}. \tag{14}$$

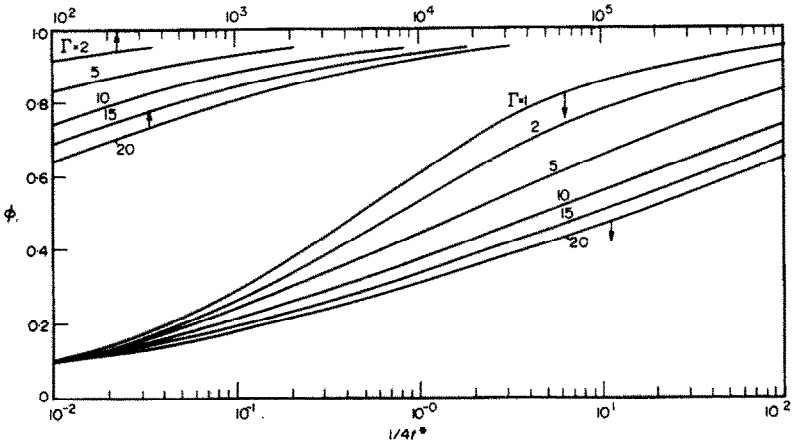

FIG. 3. Solution of equation (14).

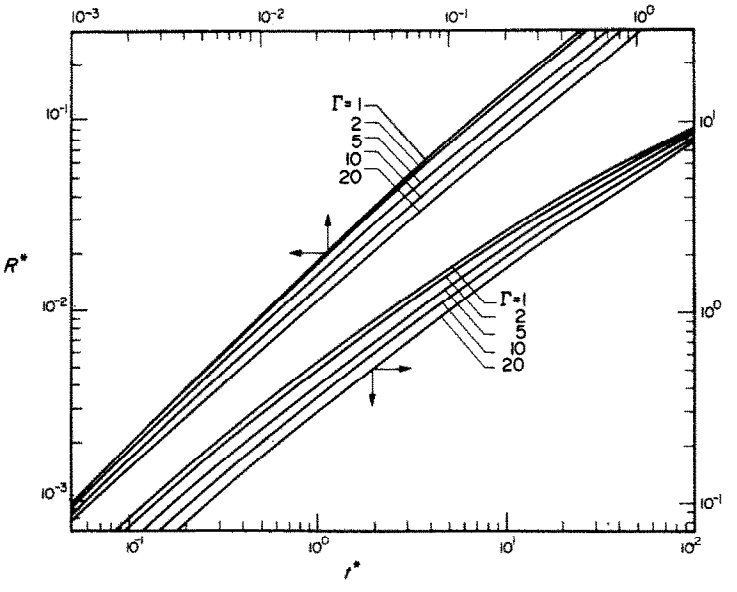

FIG. 4. Universal plot of the bubble radius versus time.

and B, "characteristic" length and time scales may be obtained and utilized to non-dimensionalize R and t thus:

$$R^* = \frac{R}{(B^2/A_*)} \quad \text{and} \quad t^* = \frac{t}{(B^2/A_*^2)}. \tag{11}$$

The system (6) and (7) finally becomes:

$$\frac{dR^*}{dt^*} = \phi \tag{12}$$

$$\frac{dR^*}{dt^*} = \frac{(1-\phi^2)}{2[1+(\Gamma-1)\phi^2]\sqrt{t^*}}. \tag{13}$$

With the initial condition $R^*(0) = 0$, the solution is obtained in the next section.

The results, for selected values of Γ up to 20, are given in graphical form in Fig. 3. These results are then utilized to obtain $R^* = R^*(t^*; \Gamma)$ by numerically integrating equation (12). The results are presented in the universal plot of Fig. 4. All lines appear to converge for both small values of t^* (inertia regime) and large values of t^* (heat-transfer regime). The maximum effect of Γ appears at intermediate values of t^*.

A universal comparison with the MRG solution is obtained by recasting it in terms of R^* and t^*. Since:

$$R^+ = \frac{A}{B^2}R = \frac{A}{A_*}R^* \equiv \beta R^* \tag{15}$$

$$t^+ = \frac{A^2}{B^2}t = \left(\frac{A}{A_*}\right)^2 t^* \equiv \beta^2 t^* \tag{16}$$

with
$$\beta \equiv \frac{A}{A_*} = \left\{\frac{\lambda\rho_v^*(P_\infty)(T_\infty - T^*(P_\infty))}{T^*(P_\infty)(P^*(T_\infty) - P_\infty)}\right\}^{1/2} \quad (17)$$

the MRG solution becomes:

$$R^*_{MRG} = \frac{2}{3\beta}\{(\beta^2 t^* + 1)^{3/2} - (\beta^2 t^*)^{3/2} - 1\}. \quad (18)$$

The numerical value of β was found to depend only on the value of Γ; hence a one-to-one comparison with the present solution is possible. The results are shown in Figs. 5 and 6. For clarity the solutions for only two values of Γ are shown. Several points may be made:

(a) For low values of $\Gamma(\Gamma = 2)$, the two solutions essentially coincide.

(b) For high values of Γ the two solutions differ by more than a factor of two. These large differences are observed only in Fig. 5 covering the low range of t^*. The two solutions converge in the high range of t^* shown in Fig. 6. This range, however, is commonly outside the range of practical interest. High Γ implies high superheat and this in turn implies large characteristic time and hence, for the range of time values of practical interest, very short dimensionless time t^* (i.e. the range covered in Fig. 5).

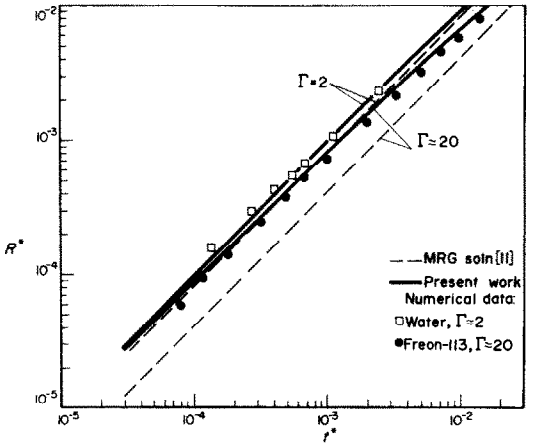

FIG. 5. A comparison of the MRG and present solutions with numerical data (discounting initial time delay due to surface tension effects) for different fluids and different conditions.

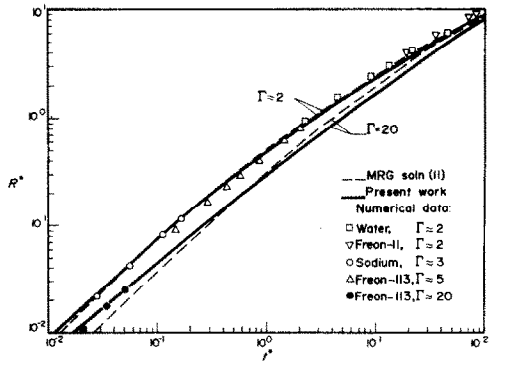

FIG. 6. A comparison of the MRG and present solutions with numerical data for different fluids and different conditions.

(c) For low t^* the present solution approaches the inertia asymptotic $R^* \sim t^*$, while the MRG solution becomes $R^*_{MRG} \sim \beta t^*$. Hence $R^* = R^*_{MRG}/\beta$ gives a measure of the maximum difference between the two solutions.

All previous experimental data happen to cover only a small range of low Γ values and have therefore been unable to demonstrate the effects pointed out above. Since details of our experimental work covering the high range of Γ will be presented separately [13], a complete numerical simulation [8] will be utilized here to support the present solution. For the high range of Γ, our Run 55-G36 with $\Gamma \simeq 20$, was simulated. The numerical results from Fig. 1 are shown, as solid circles, in Figs. 5 and 6. The present solution ($\Gamma = 20$) is quickly approached as surface tension and acceleration effects, which were retained in the numerical simulation, become negligible. Again the somewhat gradual approach of the numerical data to the present solution for the Water B1 case of Fig. 5 is due to the initially present acceleration effects. Similar numerical simulations are shown, Fig. 6, for low values of Γ. A variety of fluids and conditions were utilized to show the universally good agreement between the present solution and the numerical simulations.

Both the MRG and the present solution rely heavily on a rather fortuitous self-cancelling of the errors discussed in the formulation section. It would be expected that the MRG solution would tend to overestimate, while the present solution underestimate, ϕ. Furthermore, the present solution should provide a superior prediction of ϕ for early times. These effects are graphically presented in Fig. 7. for a typical high-Γ case. The numerical result again is accepted as the correct one. A tentative rule-of-thumb resulted from all such comparisons: The numerical ϕ values, for the slowly varying portion of the function, fall approximately midway between the MRG and the present solution.

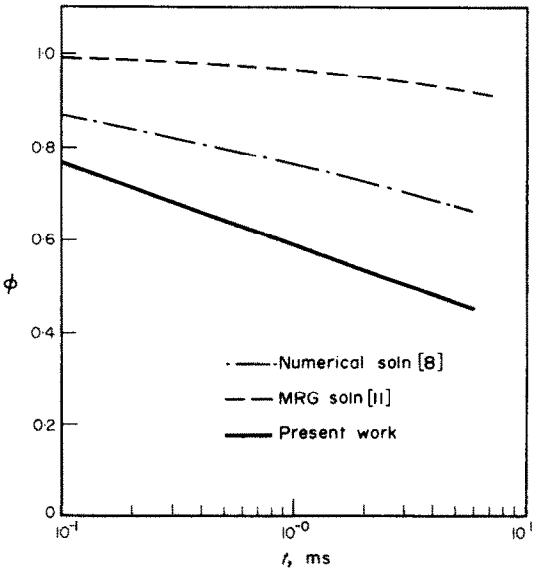

FIG. 7. A comparison of the MRG and present solutions with the numerical solution for the variation of ϕ with time.

CONCLUSIONS

The maximum error in the MRG solution is $(\beta-1)\times 100$ per cent. The value of β depends only on the initial-to-final vapor density ratio, Γ, and may be calculated from:

$$\beta=\left\{\frac{\lambda\rho_v^*(P_\infty)(T_\infty-T^*(P_\infty))}{T^*(P_\infty)(P^*(T_\infty)-P_\infty)}\right\}^{1/2}.$$

Previous comparisons with bubble growth data have failed to uncover this effect because they all happened to fall in the low Γ range. The correct solution may be read off Fig. 4, covering the mixed inertia/heat-transfer portion of the universal growth curves. For $t^*<10^{-3}$ the inertia solution, $R^*\sim t^*$, is valid within 20 per cent and for $t^*>10^2$ the heat-transfer solution $R^*=\sqrt{(t^*)}$ is valid within 15 per cent. Again the value of Γ affects these limits. The numbers given are, of course, valid for $1\leqslant\Gamma\leqslant 20$. The present as well as the MRG solution fail to accurately predict the vapor pressure (temperature) transient, which usually falls midway between the two predictions. A fortuitous error self-cancellation is responsible for the correct prediction of the radius growth curve for high-Γ conditions.

REFERENCES

1. L. Rayleigh, Pressure due to collapse of bubbles, *Phil. Mag.* **34**, 94 (1917).
2. L. E. Scriven, On the dynamics of phase growth, *Chem. Engng Sci.* **10**, 1 (1959).
3. G. Birkhoff, R. S. Margulies and W. A. Horning, Spherical bubble growth, *Physics Fluids* **1**, 201 (1958).
4. L. W. Floschuetz, C. L. Henry and A. R. Khan, Growth rates of free vapor bubbles in liquids at uniform superheats under normal and zero gravity conditions, *Int. J. Heat Mass Transfer* **12**, 1465 (1969).
5. S. G. Bankoff and H. K. Fauske, Improved prediction of critical heat flux in liquid metal pool boiling, Paper BG.1, 5th Intl. Heat Transfer Conference, Tokyo (1974).
6. H. K. Fauske, Some aspects of liquid–liquid heat transfer and explosive boiling, in Proceedings of the Fast Reactor Safety Meeting, CONF-740401-P2, 992 (1974).
7. W. J. Bornhorst and G. N. Hatsopoulos, Bubble-growth calculation without neglect of interfacial discontinuities, *J. Appl. Mech.* **34**, 847 (1967).
8. T. G. Theofanous, L. Biasi, H. S. Isbin and H. K. Fauske, Vapor bubble growth in constant and time dependent pressure fields, *Chem. Engng Sci.* **24**, 885 (1969).
9. S. J. Board and R. B. Duffey, Spherical vapour bubble growth in superheated liquids, *Chem. Engng Sci.* **26**, 263 (1971).
10. Y. C. Lien, Bubble growth rates at reduced pressure, D.Sc. Thesis, MIT (Feb. 1969).
11. B. B. Mikic, W. M. Rosenhow and P. Griffith, On bubble growth rates, *Int. J. Heat Mass Transfer* **13**, 657 (1970).
12. T. H. Bohrer, Bubble growth in highly superheated liquids, M.S. Thesis, Purdue University (May 1973).
13. T. G. Theofanous, T. Bohrer, M. Chen and P. Patel, Universal solutions for bubble growth under the influence of microlayers, *Int. J. Heat Mass Transfer*. To be published.

RELATIONS UNIVERSELLES POUR LE DEVELOPPEMENT DES BULLES

Résumé—Lorsqu'il est nettement supérieur à l'unité, le rapport des densités initiale et finale de vapeur influe fortement sur le taux de croissance des bulles de vapeur dans les régimes d'inertie et de transfert thermique inertiel. Cet effet n'est pas prévu par les formulations analytiques antérieures de Mikic, Rosenhow et Griffith. Toutes les données expérimentales publiées ont été obtenues pour de faibles valeurs de ce rapport de densités et n'ont pas permis de découvrir cette omission. La solution représentée par une courbe universelle sur la Fig. 4 ne comporte pas cette imperfection, et se trouve corroborée par les comparaisons avec des nouvelles données expérimentales et des simulations numériques détaillées.

UNIVERSELLE BEZIEHUNGEN FUR DAS BLASENWACHSTUM

Zusammenfassung—Wenn das Verhältnis der anfänglichen zur endgültigen Dampfdichte deutlich größer als eins ist, so beeinflußt es stark das Dampfblasenwachstum in den von Trägheitskraft und den von Trägheitskraft/Wärmeübergang kontrollierten Systemen. Dieser Einfluß ist in den früheren analytischen Formulierungen von Mikic, Rohsenow und Griffith nicht enthalten. Alle veröffentlichten experimentellen Daten wurden bei kleinen Werten dieses Dichteverhältnisses gewonnen und haben daher diese Auslassung nicht enthüllt. Die in der universellen Darstellung in Fig. 4 gezeigte Lösung hat diesen Nachteil nicht und wird gestützt durch Vergleiche mit neuen experimentellen Daten und detaillierten numerischen Untersuchungen.

УНИВЕРСАЛЬНЫЕ СООТНОШЕНИЯ ДЛЯ РАСЧЕТА РОСТА ПУЗЫРЬКОВ

Аннотация — Скорость роста паровых пузырьков в инерционном и инерционно-теплообменном режимах сильно зависит от отношения начальной плотности пара к конечной, если величина этого отношения намного больше единицы. Данный эффект не вытекает из известной формулы Микича, Розенау и Гриффита. Все опубликованные экспериментальные данные были получены при небольших значениях отношения плотностей, что не позволило обнаружить упущения. Решение, представленное в виде универсальной кривой на рис. 4, не обладает указанным недостатком и подтверждается новыми экспериментальными результатами и подробным численным моделированием.